



# Hydrothermal synthesis of mesoporous TiO<sub>2</sub>–ZnO nanocomposite for photocatalytic degradation of methylene blue under UV and visible light

Babak Mazinani<sup>1</sup> · Nazanin Mohamadi Zalani<sup>1</sup> · Masoud Sakaki<sup>1,2</sup> · Kazumichi Yanagisawa<sup>2</sup>

Received: 18 March 2018 / Accepted: 12 May 2018 / Published online: 23 May 2018  
© Springer Science+Business Media, LLC, part of Springer Nature 2018

## Abstract

Mesoporous ZnO–TiO<sub>2</sub> was synthesized successfully by a one-step hydrothermal procedure using titanium sulfate and Zinc nitrate hexahydrate as precursors, and Pluronic P123 as a template. The prepared ZnO–TiO<sub>2</sub> materials were heat treated at 400, 600, 800 and 1000 °C to remove the template and increase the degree of crystallization. Field emission scanning electron microscopy, wide angle X-ray diffraction, Fourier transformed infrared spectroscopy, transmission electron microscopy and N<sub>2</sub> adsorption–desorption experiments were used to characterize the synthesized powders. Comparison photocatalytic investigations for the prepared materials and commercially available P25 were carried out under identical UV and visible light to understand the effect of the achieved phases and surface area on photocatalytic rate constant and percentage degradation. Results show that the sample which was heat treated at 800 °C (S-800) presents a very high performance under visible light and around 60% of the methylene blue (MB) solution can be degraded by this catalyst in spite of its low surface area. The high efficiency of this sample under visible light can be related to its high degree of crystallinity, formation of anatase and titanium–zinc oxide phases and interfacial coupling between ZnO and TiO<sub>2</sub> nanoparticles.

## 1 Introduction

Several important industries including textile manufactures use a high amount of dyes that are generally released into the environmental water after the completion of the processes. These waste waters can lead to disastrous effects on the delicately balanced ecosystem [1, 2]. Photocatalytic degradation of the dyes in waste water have been known as an effective solution to solve the problem [3, 4].

Recently, a great deal of attention and researches have been focused on the reduction of environmental pollution by photocatalysis. Photocatalysis process is a light-activated catalytic reaction that decreases or oxidizes the organic molecules when the electron–hole pairs are produced on the surface of semiconductors by

light irradiation. ZnO and TiO<sub>2</sub> are well-known materials as solar light photocatalytic metal oxides because they exhibit great photocatalytic performance for the reduction of organic pollutants [5–11]. They show acceptable thermal, biological, and chemical stabilities besides their low price and nontoxicity [6]. Band gap of TiO<sub>2</sub> and ZnO are 3.2 and 3.37 eV, respectively, and they follow similar photodegradation mechanism [12]. Many researches have been conducted for the enhancement of the photoactivity of these semiconductors. In this regard, one of the most important improvement can be achieved by widening the photo response of these materials toward visible light which accounts for more than 90% of the solar spectrum [6, 13–15]. Various techniques have been used to make these oxides more efficient under visible light including surface modification via organic materials and band gap modification by creating oxygen vacancies, oxygen sub-stoichiometry, nanomaterials doping and transition metal doping [16]. Zhao et al. [17] found that ZnO particles on the surface of TiO<sub>2</sub> crystals can lead to the formation of coupled semiconductor system. Doped Zn on the surface of titanium oxide increases oxygen vacancies and consequently some states can be created close to conduction band of titania. The generated states provide

✉ Babak Mazinani  
b\_mazinany@alumni.iust.ac.ir

<sup>1</sup> Department of Materials Engineering, Faculty of Engineering, Malayer University, Malayer 65719-95863, Iran

<sup>2</sup> Research Laboratory of Hydrothermal Chemistry, Kochi University, Kochi 780-8520, Japan

the opportunity for the prepared composite to be active under visible light. Rahmani et al. reported the synthesis of ZnO/TiO<sub>2</sub> multilayers in which the band gap can be controlled [18].

On the other hand, photoactivity is strongly related to the surface area of semiconductors [7, 19]. Synthesis of mesoporous structure can be considered as an effective strategy to achieve high surface area, and consequently improvement of photoactivity [8, 20, 21]. Assaker et al. [15] prepared Zn–TiO<sub>2</sub> mesoporous oxides by the mechanical milling procedure. At first, they prepared mesoporous TiO<sub>2</sub> by surfactant templating mechanism, then the zinc source was mixed with the mesophase by mechanical milling. Habib et al. investigated the photoactivity of ZnO–TiO<sub>2</sub> nanocomposites under sunlight [22].

In this study, we synthesized mesoporous TiO<sub>2</sub>–ZnO composite by using Pluronic P123 via a one-step hydrothermal procedure at different calcination temperature (0, 400, 600, 800 and 1000 °C). Moreover, the influence of calcination temperature on the photocatalytic performance of the mesoporous materials was compared under UV and visible light. Interestingly, the optimum synthesis condition of the samples could improve MB degradation under visible light up to 60%. We also performed photoactivity comparison studies between commercially available P25 and the prepared materials under UV and visible light.

## 2 Experimental

### 2.1 Sample preparation

Water was deionized by using a Nano Pure System (Barnsted). The triblock copolymer Pluronic P123 (EO)<sub>20</sub>(PO)<sub>70</sub>(EO)<sub>20</sub> was purchased from Aldrich. Titanium sulfate, zinc nitrate hexahydrate, and ammonium fluoride were obtained from Merck. Figure 1 shows the synthesis flowchart of the mesoporous ZnO–TiO<sub>2</sub> materials. In this work, the samples were prepared by a modified route of previously published article [23]. In a typical synthesis, 3 g of surfactant (Pluronic P123) was dissolved in 80 g of deionized water under stirring at room temperature. Then, 3.6 g of Ti<sub>2</sub>(SO<sub>4</sub>)<sub>3</sub>, 4.46 g of Zn(NO<sub>3</sub>)<sub>6</sub>·6H<sub>2</sub>O, 0.55 g of NH<sub>4</sub>F and 3.6 g of CO(NH<sub>2</sub>)<sub>2</sub> were added dropwise. The resulting mixture was stirred for 1 h at room temperature. The achieved solution was transferred into a 100 mL Teflon-lined stainless steel autoclave, followed by hydrothermal treatment of the mixture at 180 °C for 6 h. After the hydrothermal process, the white precipitate was centrifuged and washed with distilled water and ethanol for three times. The final precipitate was dried at 80 °C for

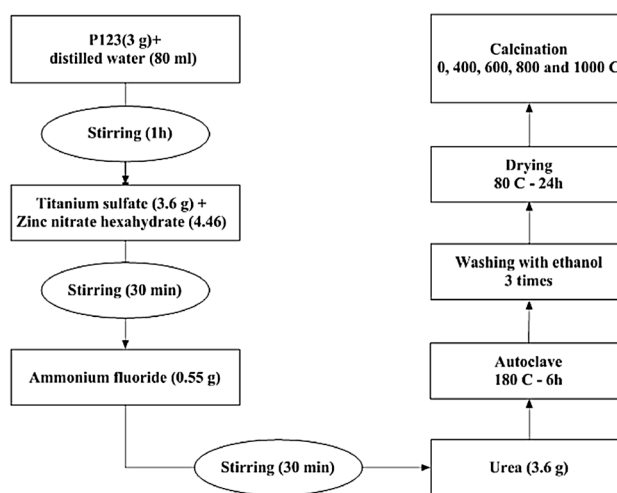


Fig. 1 Flowchart of the preparation steps of the samples

24 h. Finally, the prepared powder was calcined in air at different temperatures (0, 400, 600, 800, 1000 °C) for 2 h.

### 2.2 Characterization

The samples were characterized by X-ray diffraction (XRD) using a Unisantis instrument model XMD300. The equipment was operated at 45 kV with Cu K $\alpha$  radiation (1.5405 Å), and the diffractometer was functioned at a scan rate of 0.04°/s over a 2 $\theta$  range of 20°–70°. Field emission scanning electron microscope (FESEM- Tescan Mira) was employed to observe the morphology of the prepared materials equipped with an energy-dispersive X-ray analysis (EDX). The N<sub>2</sub> adsorption–desorption isotherms were measured using a Belsorb-mini II instrument. Samples were thoroughly degassed at 100 °C for 10 h before the adsorption measurements. Fourier transformed infrared spectroscopy (FTIR) analysis of the materials were carried out using a WQF-510 equipment and spectra were recorded in the 400–4000 cm<sup>-1</sup> region. Transmission electron microscopy (TEM, 2000FX2, JEOL, Japan) was used for the morphological investigation.

### 2.3 Photocatalytic and band-gap measurements

Methylene blue (MB) was chosen as an organic compound to analyze the photocatalytic efficiency of the prepared materials under UV light (mercury lamp 125 W) and visible light (200 W) irradiation about 10 cm above the reaction container. In a typical experiment, 0.1 g of the powder was dispersed in 40 mL MB solution having a concentration 10 ppm. The mixture was first reacted for 60 min under dark condition to ensure the establishment of an adsorption–desorption equilibrium. At each periods of time (30 min under

UV light and visible light), 3 mL of the mixture was separated. The concentration spectra of the mixtures were recorded using UV–vis spectrometry (at 625 nm) after centrifugation to remove the particles (5000 rpm).

The band gap ( $E_g$ ) values were determined using the following direct transition equation.

$$\alpha h\nu = (h\nu - E_g)^{0.5} \quad (1)$$

where  $\alpha$  is the optical absorption coefficient,  $h$  is Planck's constant,  $\nu$  is the frequency ( $h\nu = 1240/\text{wavelength}$ ),  $E_g$  is the direct band gap, and  $E_d$  is a constant [24]. By plotting  $(\alpha h\nu)^2$  as a function of the photon energy ( $h\nu$ ) and extrapolating the linear portion of the curve to a value of zero, band gap ( $E_g$ ) was calculated.

### 3 Results and discussion

XRD patterns of the samples are shown in Fig. 2a. As it can be seen, there are large differences among the peak intensities of the samples because of different degree of crystallinity. It is well known that higher calcination temperature can improve crystallinity [7]. The three samples of S-0, S-400 and S-600 exhibit similar XRD patterns well assigned to the anatase crystalline phase of  $\text{TiO}_2$  (JCPDS Ref No.: 01-073-1764) and wurtzite  $\text{ZnO}$  (JCPDS Ref No.: 01-079-0207). At a higher calcination temperature (800 °C), the new diffraction peaks can be indexed to  $\text{TiO}_2 \cdot 2\text{ZnO}$  (JCPDS Ref No.: 01-077-0014) besides anatase and wurtzite crystals. Interestingly, Anatase is the only detected  $\text{TiO}_2$  crystal phase at 800 °C which can be related to inhibition of the anatase–rutile phase transformation with addition of  $\text{ZnO}$  [25]. When the S-1000 sample was calcined at 1000 °C, phase transformation from anatase to rutile took place.

Diffraction peaks of rutile and  $\text{TiO}_2 \cdot 2\text{ZnO}$  can be observed clearly in S-1000 sample. Although it is reported that titanium–zinc oxide phase ( $2\text{ZnO} \cdot \text{TiO}_2$ ) with a spinel structure can be formed at 1050–1100 °C, its characteristic peaks was detected at S-800 and S-1000 [26]. Khalyavka et al. [27] have mentioned that the titanium–zinc oxide nanocomposites show higher photoactivity compared with  $\text{ZnO}$  and  $\text{TiO}_2$ . Moreover, based on scherrer equation [24] the crystal sizes of the prepared samples calculated and are presented in Table 1. It can be seen that the higher calcination temperature causes a growth in crystal size of the materials.

Figure 2b shows the FT-IR spectra of typical as-prepared and calcined samples. The broad adsorption bands in the range of 3000–3800  $\text{cm}^{-1}$  are assigned to the stretching vibrations of the OH group [28]. Broad peaks emerge below 800  $\text{cm}^{-1}$ , which are due to the vibration of metal oxide structures. The presence of a peak around 650 and 800  $\text{cm}^{-1}$  can be related to symmetric stretching vibration of the Ti–O–Ti and vibration mode of Zn–O–Ti bands. The peak at  $\sim 1450 \text{ cm}^{-1}$  was devoted to the vibration mode of Ti–O and Ti–O–C. The Ti–O–C bands can be from the interaction between the Ti–O network and the P123 [29–32].

EDX mapping of Zn and Ti was performed on S-0 (Fig. 3a–c). A homogeneous distribution of Zn and Ti can be confirmed based on elemental mapping images. TEM image illustrated in Fig. 3d shows that  $\text{TiO}_2$ – $\text{ZnO}$  nanoparticles are ultrafine.

The  $\text{N}_2$  adsorption–desorption isotherms of the samples are displayed in Fig. 4 and tabulated in Table 1, which shows the specific surface area, mean pore size and pore volume of the samples. All isotherms resembled the IV isotherm type, which is a characteristic of mesoporous materials typically according to IUPAC classification [33]. It should be noted that, based on this hydrothermal synthesis procedure,

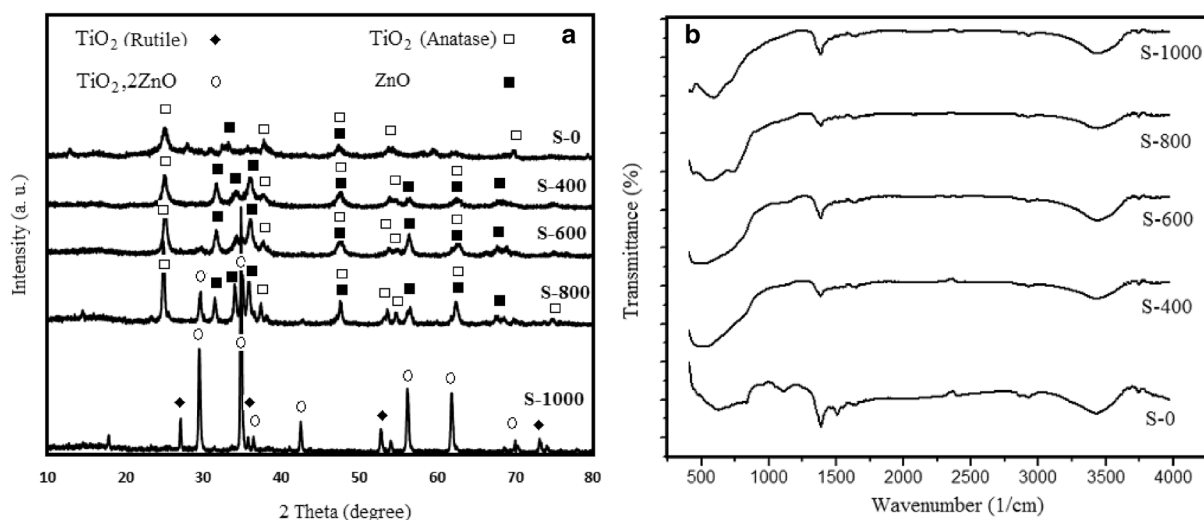


Fig. 2 XRD patterns (a) and FTIR spectra (b) of the samples

**Table 1** Textural properties, photocatalytic efficiency and band gap energy of the prepared materials

Sample	UV light		Visible light		$S_{\text{BET}}$ ( $\text{m}^2/\text{g}$ ) <sup>c</sup>	$V_p$ ( $\text{cm}^3/\text{g}$ ) <sup>d</sup>	$D_p$ (nm) <sup>e</sup>	Crystal size (nm)	Band gap (eV)
	Degradation <sup>a</sup> (%)	$K$ ( $\text{min}^{-1}$ ) <sup>b</sup>	Degradation (%)	$K$ ( $\text{min}^{-1}$ )					
S-0	54.8	0.0074	14	0.0012	88.41	0.52	23.8	8.1	3.36
S-400	55.6	0.0042	26.6	0.0023	63.6	0.24	15.1	9.4	3.25
S-600	42.2	0.0038	36.4	0.0036	31.5	0.14	18.1	12.6	3.19
S-800	58.1	0.0077	58.5	0.0069	18.2	0.08	18.2	20.1	3.03
S-1000	12.6	0.001	10.3	0.0008	–	–	–	27.5	3.01
P25	61.2	0.0087	31.7	0.0032	–	–	–	–	3.4

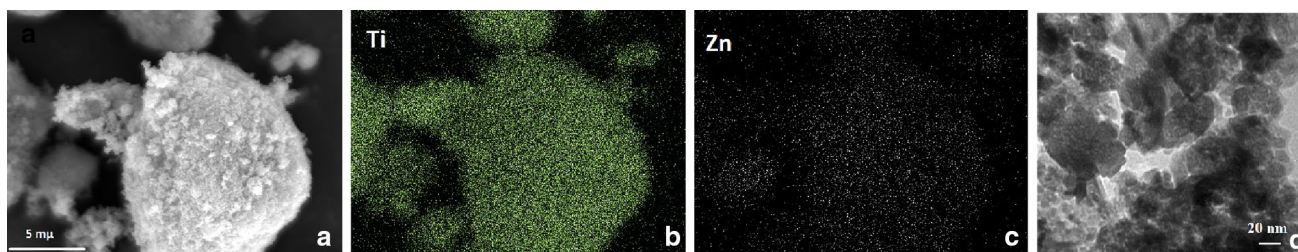
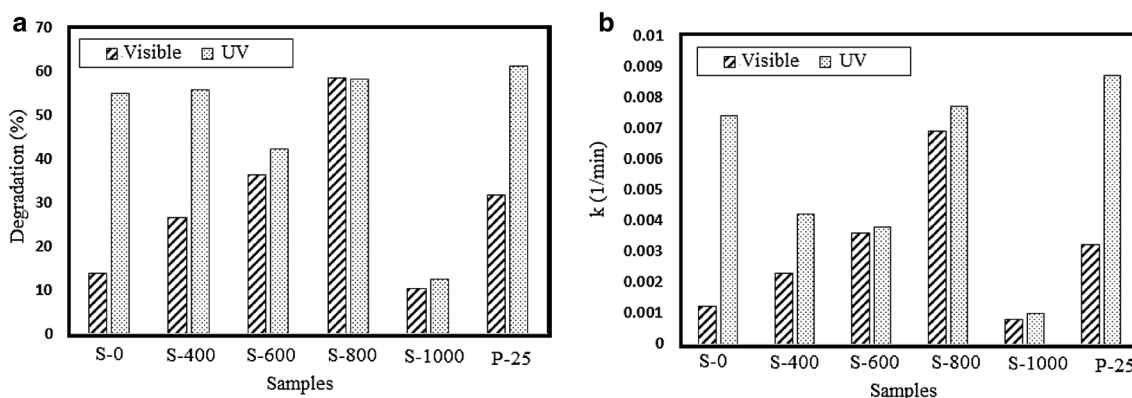
<sup>a</sup>Percentage degradation calculated based on Eq. 3

<sup>b</sup>Rate constant calculated based on Eq. 2

<sup>c</sup>Surface area calculated by a BET method

<sup>d</sup>Total pore volume

<sup>e</sup>Pore diameter calculated by a BJH method

**Fig. 3** SEM image with EDX elemental mapping (a–c) and TEM image (d) for S-0**Fig. 4**  $\text{N}_2$  adsorption–desorption isotherms of the prepared samples

mesoporous structure can also be achieved without using of P123. However, the existence of P123 have improved the surface area and pore volume dramatically. As it can be seen in Table 1, a decrease in surface area and pore volume takes place at higher calcination temperatures. Generally, because the photocatalytic reactions of heterogeneous materials are happened on the surface of reactants, a higher surface area, pore sizes, and pore volume can improve the photocatalytic

performance by creating more active sites for the photochemical process [6, 7, 9, 11].

It should be mentioned that the rate of degradation obeys pseudo-first-order kinetics. The initial reaction rate constants can be measured based on the formula

$$-\ln(C/C_0) = kt \quad (2)$$

where  $C_0$  is the initial concentration of the dye,  $C$  is the concentration after time  $t$  and  $k$  is the constant of the degradation.

Degradation of MB can be a result of surface adsorption or photodegradation. To assess the photodegradation of the dye, the suspension was stirred for half an hour in the dark condition in advance in order to reach the adsorption–desorption equilibrium. Estimated  $k$  for the samples according to Fig. 5 is shown in Table 1 and Fig. 6b under both UV and visible conditions. The photocatalytic efficiency of the commercial photocatalyst Evonik P25 was also measured under the same procedure. As it can be seen in Fig. 5, increasing of calcination temperature until 800 °C has promoted the reaction rate of the samples under both visible and UV light. Higher calcination temperatures could improve the degree of crystallinity and effectively eliminate the bulk defect positions for the recombination of the photo-induced electron–hole pairs [7, 9, 34]. At very high calcination temperature (1000 °C), reaction rate constant of sample has dropped dramatically (Table 1; Fig. 6) because of

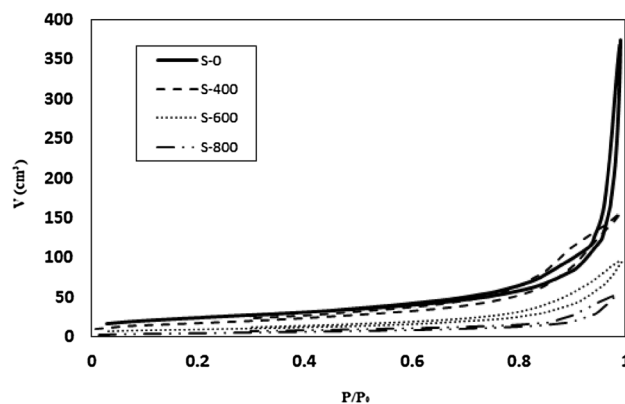


Fig. 6 MB degradation percent (a) and reaction rate constant (b) of the materials under UV and visible light

formation of rutile phase (Fig. 2a). Although kinetic rate of P25 is higher than of all samples under UV light, it is around half-larger than S-800 under visible light. It is proved that

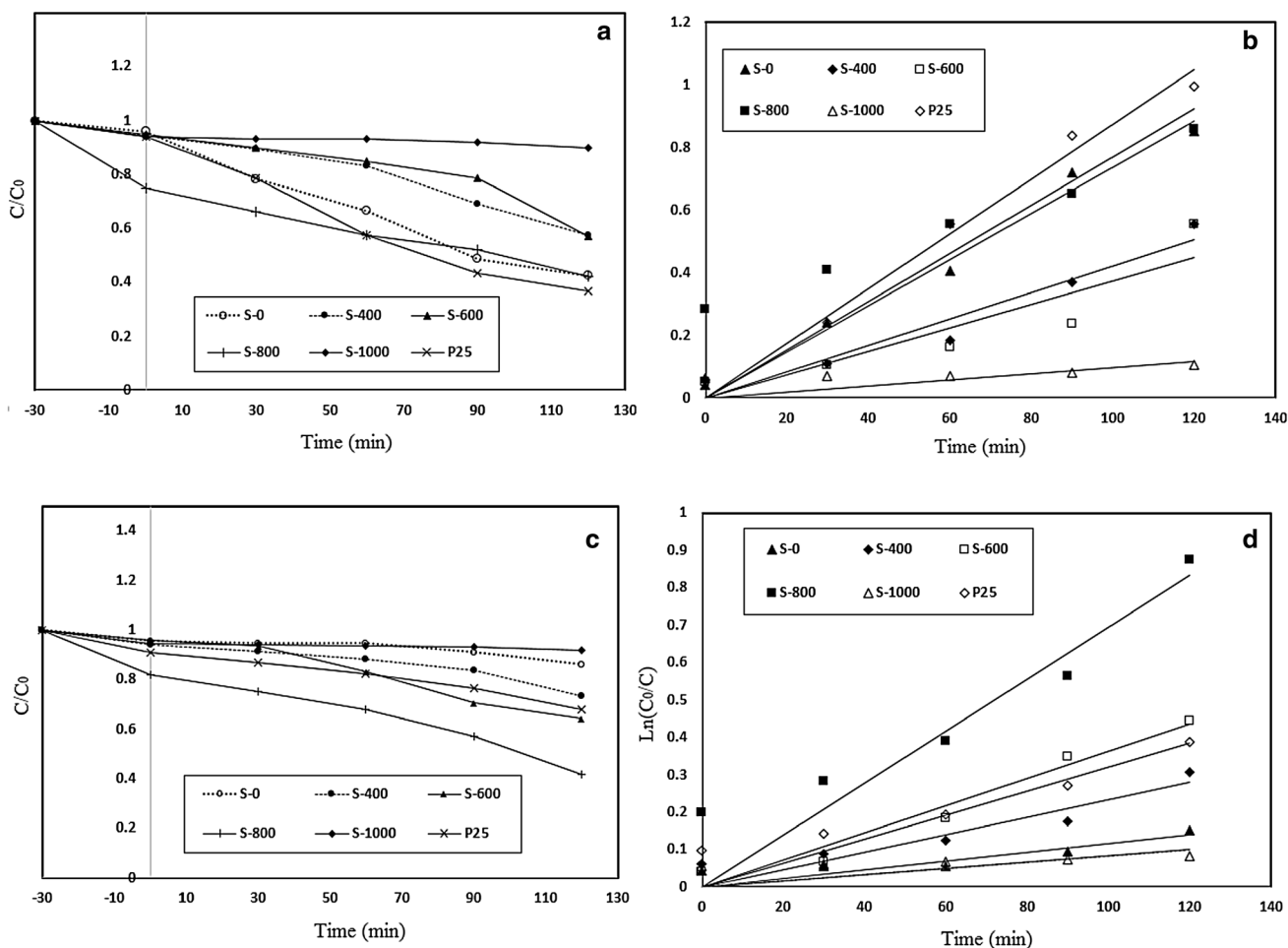


Fig. 5 Photocatalytic activity (a and c) and degradation kinetics (b and d) of the materials under UV light (a and b) and visible light (c and d)

interfacial coupling between ZnO and TiO<sub>2</sub> nanoparticles decreases the band gap of TiO<sub>2</sub> and consequently makes it visible light active for the degradation of dyes [35]. Because of the combination of high degree of crystallinity, formation of anatase and titanium-zinc oxide phases and a narrow band gap (Table 1) of the composite, the sample S-800 shows an excellent performance under visible light.

The percentage degradation of the materials was evaluated according to the following equation:

$$\text{Degradation}(\%) = \left( \frac{C_0 - C_t}{C_0} \right) \times 100 \quad (3)$$

where  $C_0$  is the initial concentration of MB before irradiation, and  $C_t$  is the dye concentration at time  $t$ . As it can be seen in Table 1 and Fig. 6a, S-800 shows the highest degradation (around 60%) of MB under visible light. In fact, a similar trend can be detected for percentage degradation of MB and reaction rate constant of the samples.

## 4 Summary

Mesoporous structures of ZnO–TiO<sub>2</sub> were prepared through the hydrothermal method. The characterization results show that the existence of ZnO nanoparticles inhibit phase transformation of TiO<sub>2</sub> from anatase to rutile structure up to at least 800 °C. Energy-dispersive X-ray analysis mapping of the prepared samples demonstrate the dispersion of Zn and Ti elements homogeneously. The highest efficiency of photocatalytic activity in terms of percentage degradation of MB and reaction rate constant can be achieved for the samples at calcined at 800 °C. Photoactivity of the sample which heat treated at 800 °C, was around twice as big as commercial P25 under visible light.

**Acknowledgements** This work has been supported by the Center for International Scientific Studies & Collaboration (CISSC). Further, we are also grateful for the kind collaboration of Kochi University (Japan).

## References

1. P. Cooper, *Colour in Dyehouse Effluent* (Society of dyers and colourists, Bradford, 1995)
2. Y.M. Slokar, A.M. Le Marechal, *Dye. Pigment.* **37**, 335 (1998)
3. F. Han, V.S.R. Kambala, M. Srinivasan, D. Rajarathnam, R. Naidu, *Appl. Catal. A Gen.* **359**, 25 (2009)
4. B. Mirtaheri, M. Shokouhimehr, A. Beitollahi, *J. Sol-Gel. Sci. Technol.* **82**, 148 (2017)
5. J. Strunk, K. Köhler, X. Xia, M. Muhler, *Surf. Sci.* **603**, 1776 (2009)
6. A. Taufik, A. Albert, R. Saleh, *J. Photochem. Photobiol. A Chem.* **344**, 149 (2017)
7. B. Mazinani, A.K. Masrom, A. Beitollahi, R. Luque, *Ceram. Int.* **40**, 11525 (2014)
8. B. Mazinani, A. Beitollahi, A.K. Masrom, N. Yahya, T.S.Y. Choong, S.M. Ibrahim, J. Javadpour, *Res. Chem. Intermed.* **38**, 1733 (2012)
9. B. Haghightazadeh, M.S. Mazinani, L. Asl, Bakhtiari, *Desalin. Water Treat.* **80**, 156–163 (2017)
10. S.M. Ibrahim, A.K. Masrom, B. Mazinani, S. Radiman, F.M. Jamil, A. Beitollahi, N. Negishi, N. Yahya, *Res. Chem. Intermed.* **39**, 1003 (2013)
11. A. Mazinani, S. Beitollahi, A.K. Radiman, S.M. Masrom, J. Ibrahim, F.M.D. Javadpour, Jamil, *J. Alloys Compd.* **519**, 72 (2012)
12. S. Logothetidis, A. Laskarakis, S. Kassavetis, S. Lousinian, C. Gravalidis, G. Kiriakidis, *Thin Solid Films* **516**, 1345 (2008)
13. Y. Liu, S. Wei, W. Gao, *J. Hazard. Mater.* **287**, 59 (2015)
14. R.S. Mane, W.J. Lee, H.M. Pathan, S.-H. Han, *J. Phys. Chem. B* **109**, 24254 (2005)
15. K. Assaker, B. Lebeau, L. Michelin, P. Gaudin, C. Carteret, L. Vidal, M. Bonne, J.L. Blin, *J. Alloys Compd.* **649**, 1 (2015)
16. S. Rehman, R. Ullah, A.M. Butt, N.D. Gohar, *J. Hazard. Mater.* **170**, 560 (2009)
17. Y. Zhao, C. Li, X. Liu, F. Gu, H.L. Du, L. Shi, *Appl. Catal. B Environ.* **79**, 208 (2008)
18. F. Rahmani, M. Ardyanian, *J. Mater. Sci. Mater. Electron.* **1**, 4285 (2018)
19. L. Jing, Z. Xu, X. Sun, J. Shang, W. Cai, *Appl. Surf. Sci.* **180**, 308 (2001)
20. T. Wagner, T. Waitz, J. Roggenbuck, M. Fröba, C.-D. Kohl, M. Tiemann, *Thin Solid Films* **515**, 8360 (2007)
21. F. Chen, Y.B. Huang, R.A. Cheng, Caruso, *Adv. Mater.* **21**, 2206 (2009)
22. M.A. Habib, M.T. Shahadat, N.M. Bahadur, I.M.I. Ismail, A.J. Mahmood, *Int. Nano Lett.* **3**, 5 (2013)
23. Y. Wang, S. Zhu, X. Chen, Y. Tang, Y. Jiang, Z. Peng, H. Wang, *Appl. Surf. Sci.* **307**, 263 (2014)
24. P. Scherrer, *Nachr. Ges. Wiss. Göttingen* **2**, 98 (1918)
25. M.S.P. Francisco, V.R. Mastelaro, *Chem. Mater.* **14**, 2514 (2002)
26. G. Göndöz, *Chemistry, Materials, and Properties of Surface Coatings: Traditional and Evolving Technologies* (DEStech Publications, Inc, Lancaster, 2015)
27. T.A. Khalyavka, E.I. Kapinus, T.I. Viktorova, N.N. Tsyba, *Theor. Exp. Chem.* **45**, 223 (2009)
28. V.G. Deshmane, R.Y. Abrokwhah, D. Kuila, *J. Mol. Catal. A Chem.* **408**, 202 (2015)
29. J. Tian, L. Chen, Y. Yin, X. Wang, J. Dai, Z. Zhu, X. Liu, P. Wu, *Surf. Coat. Technol.* **204**, 205 (2009)
30. K. Karthik, S.K. Pandian, N.V. Jaya, *Appl. Surf. Sci.* **256**, 6829 (2010)
31. J. Wang, J. Li, Y. Xie, C. Li, G. Han, L. Zhang, R. Xu, X. Zhang, *J. Environ. Manage.* **91**, 677 (2010)
32. S. Moradi, P. Aberoomand Azar, S. Raeis Farshid, S. Abedini, M.H. Khorrami, Givianrad, *Int. J. Chem. Eng.* (2012). <https://doi.org/10.1155/2012/215373>
33. K.S.W. Sing, *Pure Appl. Chem.* **57**, 603 (1985)
34. B. Mazinani, A. Beitollahi, A.K. Masrom, N. Yahya, T.S.Y. Choong, S.M. Ibrahim, J. Javadpour, *Res. Chem. Intermed.* **38**, 373 (2012)
35. H. Chen, S. Zhang, J. Hu, Li, *J. Phys. Chem. C* **112**, 117 (2008)